Supporting Information

High quantum yield pure blue emission and fast proton conduction from an indium−metal−organic framework

Lu Zhai,[a, b] Jin−Wei Yu,[a] Jin Zhang,[a] Wen−Wei Zhang,*[b] Lifeng Wang, [c] Xiao−Ming Ren*[a,b,d]

[a]State Key Laboratory of Materials−Oriented Chemical Engineering and College of Chemistry & Molecular Engineering, Nanjing Tech University, Nanjing 211816, P. R. China

[b]State Key Laboratory of Coordination Chemistry, School of Chemistry and Chemical Engineering, Nanjing University, Nanjing 210023 P. R. China
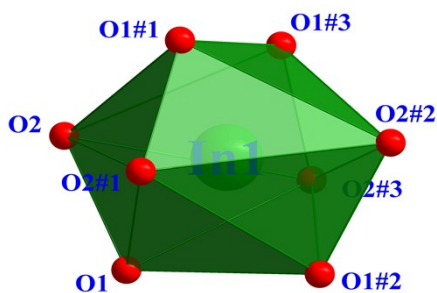
[c]Institute for Frontier Materials (IFM), Deakin University, 75 Pigdons Road, Waurn Ponds, Victoria 3216, Australia

[d]College of Materials Science & Engineering, Nanjing Tech University, Nanjing 211816, P. R. China

E−mail: wwzhang@nju.edu.cn (WWZ)

　　　xmren@njtech.edu.cn (XMR)

Table S1: Selected bond lengths (Å) and angles (º) in crystal of **1** at 298 K

Bond lengths/Å			
In1−O1	2.176(4)	In1−O1#1	2.176(4)
In1−O1#2	2.176(4)	In1−O1#3	2.176(4)
In1−O2	2.422(5)	In1−O2#1	2.422(5)
In1−O2#2	2.422(5)	In1−O2#3	2.422(5)

Bond angles/º			
O1−In1−O1#1	124.76(12)	O1#1−In1−O2#1	55.24(12)
O1−In1−O1#2	81.94(19)	O2#2−In1−O2#1	90.67(3)
O1−In1−O1#3	124.76(12)	O2#2−In1−O2#3	90.67(3)
O1#1−In1−O1#2	124.76(12)	O2−In1−O2#2	167.634
O1#1−In1−O1#3	124.76(12)	O1#1−In1−O2#3	137.154
O1#2−In1−O1#3	81.94(19)	O1#2−In1−O2#1	85.335
O2−In1−O2#1	90.67(3)	O1#2−In1−O2#2	55.213
O2−In1−O2#3	90.67(3)	O1#3−In1−O2#3	55.213

symmetry code: #1 = 1−x, 1−y, 1/2−z; #2 = 1−x, 1−y, z; #3 = y, x, 1/2−z.
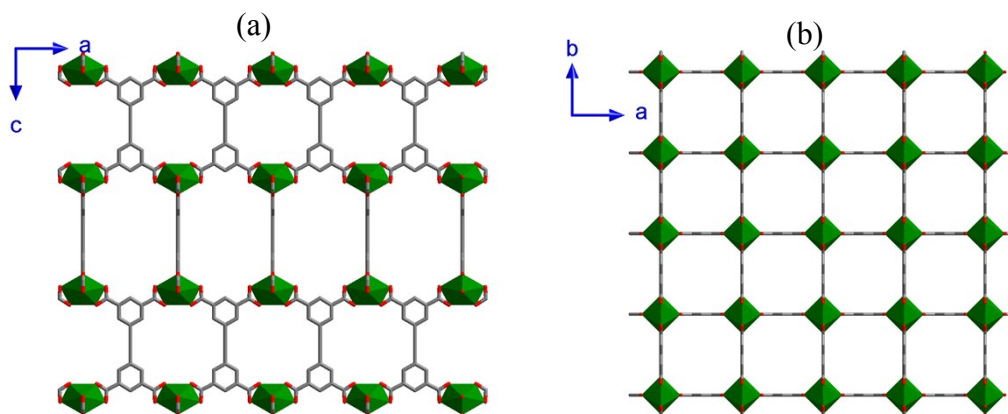
1. Crystal structure

Figure S1. Framework of metal−carboxylate viewed along (a) [010] and (b) [001] directions (Hydrogen atoms and guest molecules are omitted for clarity).
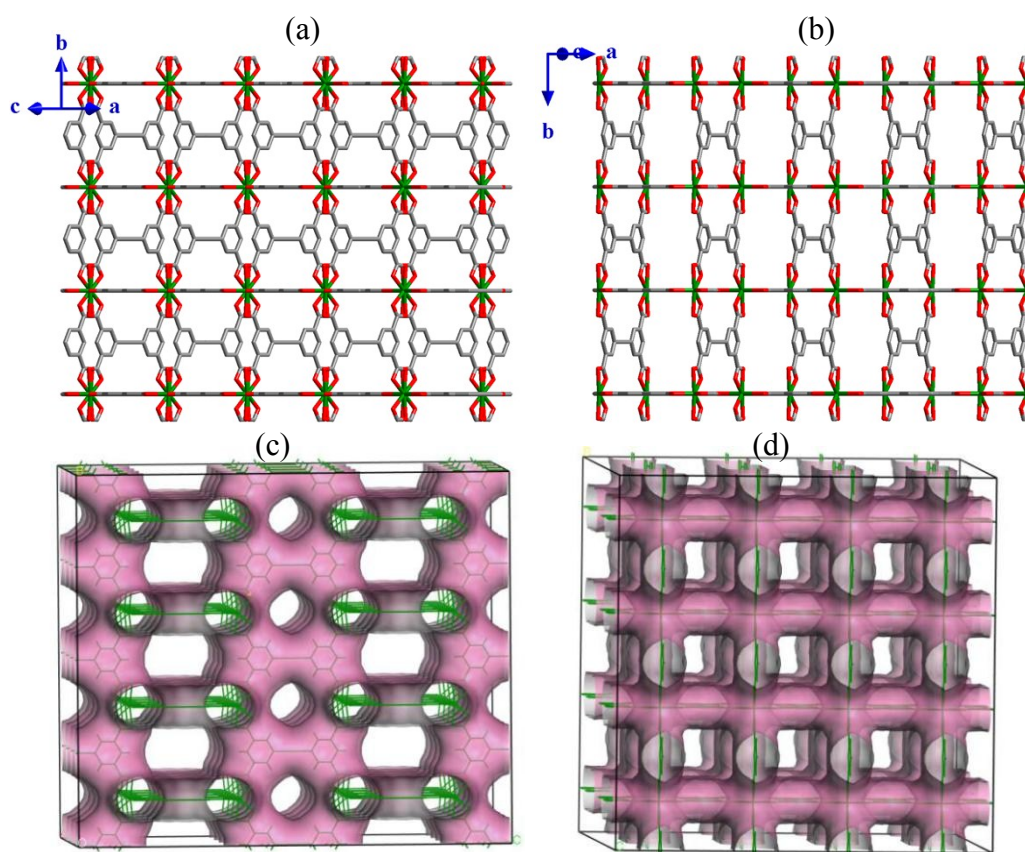

Figure S2. The structure of **1** viewed along (a) [201] direction and (b) [10−1] direction and (c, d) solvent accessible pores in **1** simulated using Materials Studio 6.0 (Hydrogen atoms and guest molecules are omitted for clarity).

2. Characterizations

2.1 Phase purity

The powder X–ray diffraction (PXRD) experiments for **1** was carried out carefully to check phase purity at room temperature. The patterns showed that the main peaks of the synthesized MOF were closely consistent with that of the simulation from the single–crystal X–ray diffraction data, which imply high quality of the obtained products (Figure S3). The difference in reflection intensities is probably due to the preferred orientation effects.
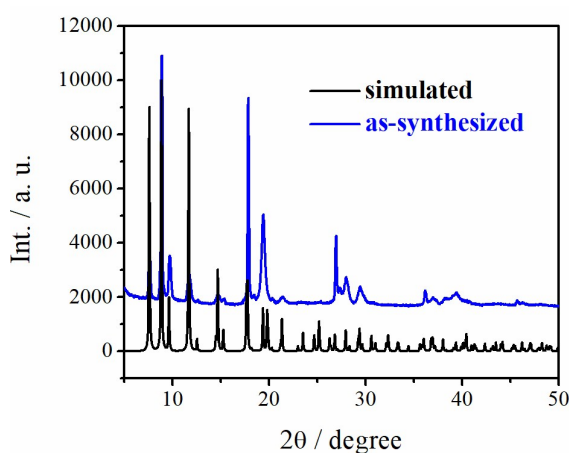

Figure S3. PXRD patterns of **1** at ambient temperature.
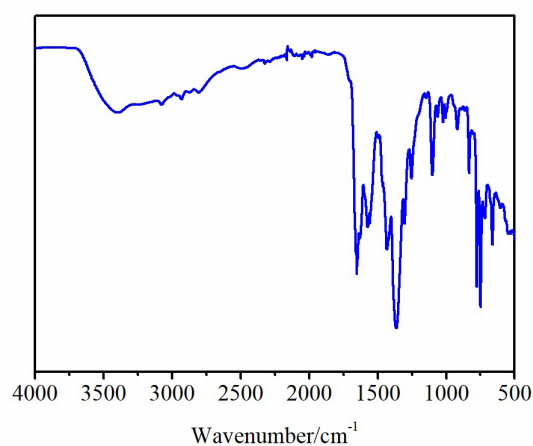
2.2 IR Spectrum

Figure S4. IR spectrum of **1** recorded using KBr pellet.

2.3 Thermal stability and water stability

TGA was employed to investigate the thermal stability of **1**. Figure S5 shows the results obtained. The empirical formula can be further confirmed by the TGA result. During heating from 30 to 212 °C, the first step in the TGA curve with a 30.64% weight loss was related to the escape of five water and one DMF molecules together with one $[(CH_3)_2NH_2]^+$ counterion presented in the channels of **1** (calc.:31.02%). In the temperature range of 212–390 °C, no obvious weight loss was further observed, which confirms the stability of the framework. With further heating, a sharp weight loss was observed, due to the decomposition of the framework. The final residue was In_2O_3.
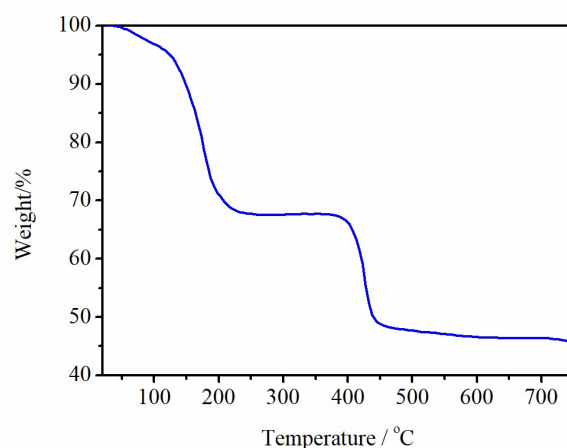

Figure S5. TG plot of **1** in the ranges of 28–800 °C.

3. Absorption and emission spectra

Figure S6 depicts the UV–visible absorption spectra of **1** together with the ligand H_4EBTC in solid state at room temperature, both show two main absorption bands in the ranges of 200–400 nm. In the case of **1**, the electronic absorption spectrum shows low energy absorption bands at ca. 302 nm (317 nm for ligand) and higher energy absorption bands at ca. 222 nm (280 nm for ligand) attributed to the intraligand $\pi \rightarrow \pi^*$ electron transitions within the aromatic rings and the carboxyl groups, as well as the $n \rightarrow \pi^*$ electron transitions in the carboxyl groups. The electronic absorption spectra of **1** compared with ligands are blue–shifted, for the metal perturbed intraligand $\pi \rightarrow \pi^*$ transition. The optical band gap is calculated to be 3.64 eV which is consistent with the observation that the crystal of **1** exhibits colorless under daylight.

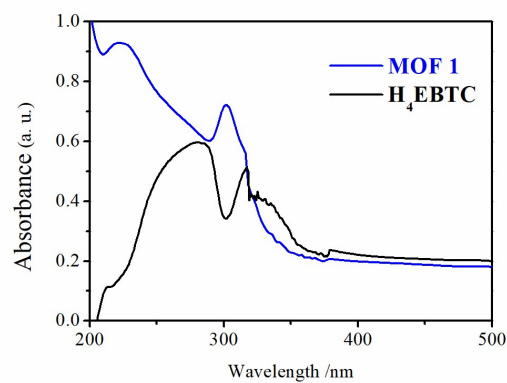**Figure S6.** UV−vis absorption spectra for **1** (blue) and the H$_4$EBTC ligand (black).
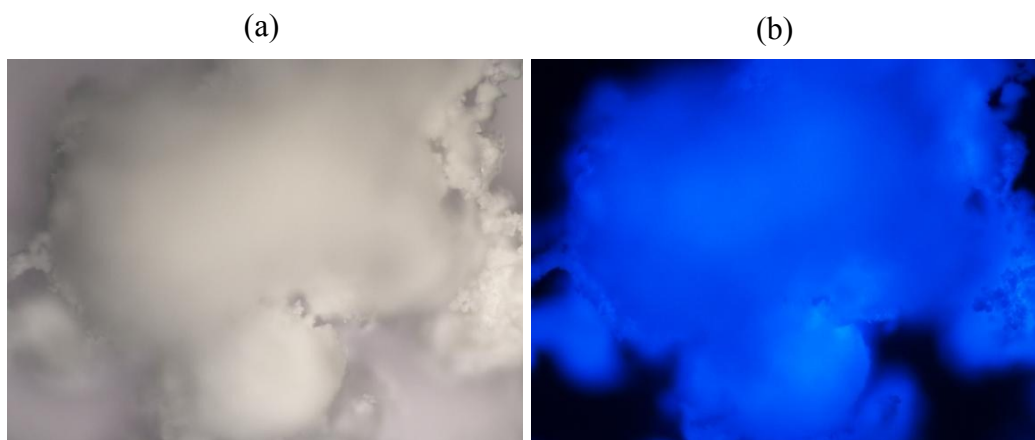
(a)   (b)

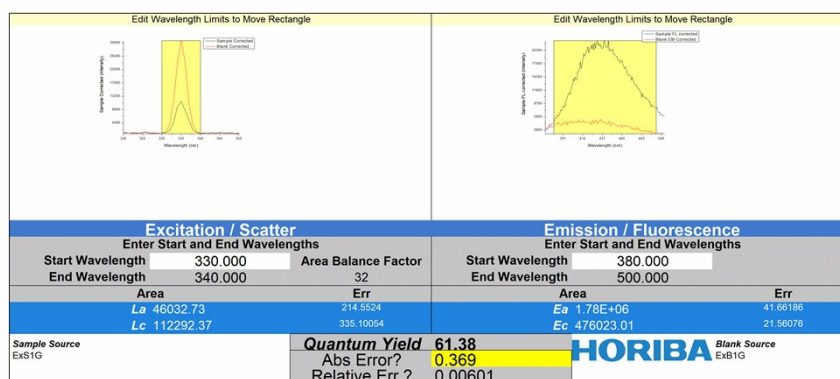**Figure S7**. Powder samples of **1** under (a) daylight and (b) UV light (λ = 330–380 nm), respectively.

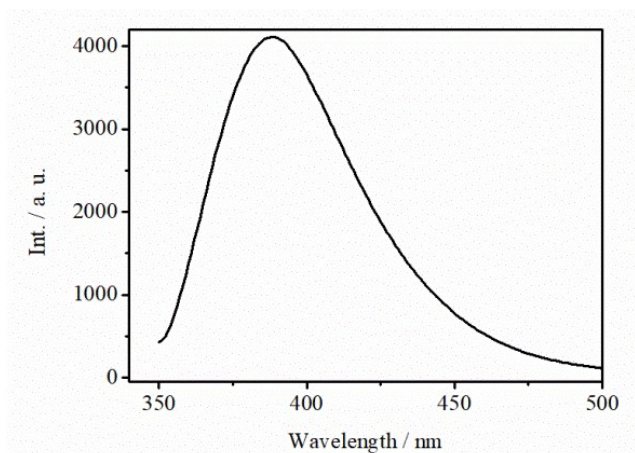**Figure S8**. Solid state quantum yield determination result of **1** at ambient condition.

Figure S9. Solid–state PL spectra of H_4EBTC (λ_{ex}= 278 nm) at room temperature.

The variable temperature emission spectra in solid state are subsequently investigated in the range of 10–300 K (Figure S10). Upon cooling from 300 to 10 K, the emission intensity enhances by ~9 times due to that the thermal activation of non–radiative relaxation process being suppressed at low temperature. Noticeably, a new band comes into view in the regime around 530 nm in the low temperature emission spectra. The analogous phenomenon has also been observed previously in other coordination polymers containing the partially and fully deprotonated H_4EBTC ligand,[1] and the new emission band observed in low-temperature probably attributed to the emission of the lattice defects.[2]
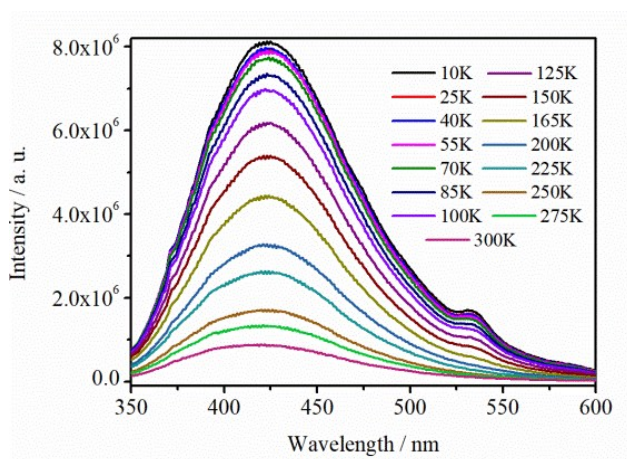
Figure S10. Temperature–dependent solid state emission spectra of **1** in the range of 10–300 K.

4. Proton conductance

Proton transfer activation energy, E_a, was estimated from the following equation,

$$\ln(\sigma T) = \ln A - \frac{E_a}{k_B T}$$

where the symbols σ, A, E_a and k_B represent the proton conductivity, the pre–exponential factor, the proton–transport activation energy and Boltzmann constant, respectively.

Figure S11. (a) Humidity–dependent proton conductivity at 25 °C (b) Nyquist plots from AC impedance data of **1** at 25 °C and humidity variation from 60% to 98%, where the measurements were performed using the powdered pellet (c) the AC impedance spectra of **1** at 25 °C and the humidity variation from 60% to 95%, where the measurements were made using the interdigital electrodes.
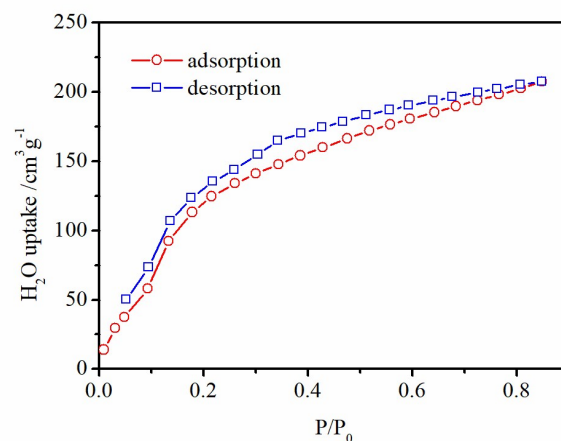
Figure S12. Water vapor adsorption isotherms of **1** at 20 °C as a function of P/P_0.

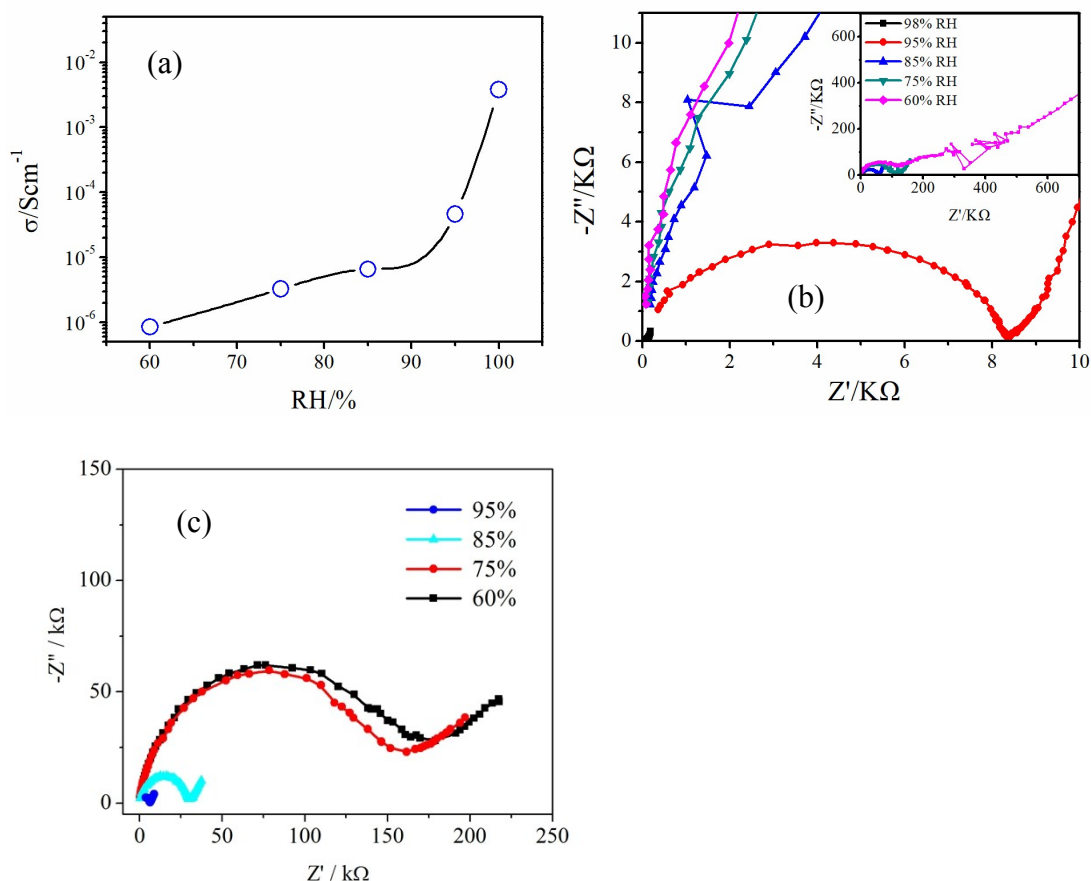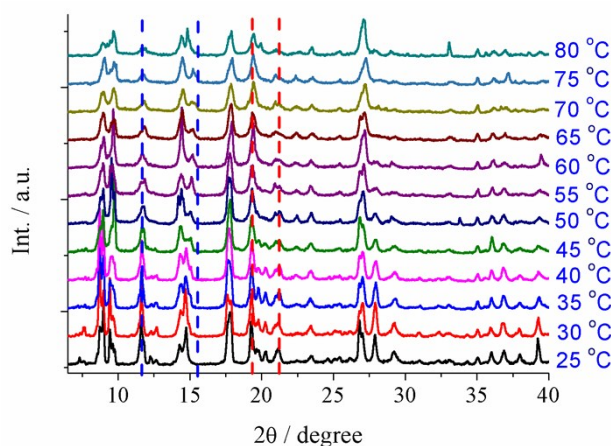**Figure S13.** Variable–temperature PXRD patterns of **1**.

Table S2: High quantum yield blue emitting MOFs reported to date

MOF	QY/%	λ_{ex}/nm	λ_{em}/nm	Reference
Zn(idpa)(py)	22.5	365	420	*Inorg. Chim. Acta.,* 2016, 453, 8–15.
[Cd(idpa)(bpp)]·nH₂O	28.1	365	435	*CrystEngComm.,* 2015, 17 9155–9166.
[Zn(idpa)(phen)(H₂O)]·nH₂O	39.8	340	423	*CrystEngComm.,* 2015, 17 9155–9166.
Zr₆(OH)₆(ndc)₆	30	371	400	*Phys. Chem. Chem. Phys.,* 2016,18, 5112–5120.
{(H₂NMe₂)[Cd(TTAA)]}·2H₂O	40.3	318	432	*Chem. Commun.,* 2012, 48, 531–533.
ZJU-28	-	365	415	*Adv. Funct. Mater.,* 2015, 25, 4796–4802.
LMOF-401	57.7	360	459	*Cryst. Growth Des.,* 2016, 16, 4178−4182.
CuP6	62	375	465	*J. Phys. Chem. C.,* 2017, 121, 23072–23079.
In-MOF	61.4	335	406	This work

Table S3: Proton conductivity values of **1** in comparison with high–performing water–mediated proton conducting MOFs (pelletized powders)

Material	σ/S cm^{-1}	Conditions	E_a/eV	Ref.
In-MOF	3.49×10^{-3}	25°C, 98% RH	0.105	This work
	9.22×10^{-3}	65°C, 98% RH	0.17	
ZrP	8.10×10^{-3}	25°C, 100% RH	0.30	*J. Am. Chem. Soc.* **2018**,
	1.21×10^{-2}	90°C, 95% RH		140, 6146–6155
MIT-25	6.80×10^{-5}	25°C, 95% RH	0.40	*J. Am. Chem. Soc.* **2018**,
	5.10×10^{-4}	75°C, 95% RH		140, 2016–2019
KAUST-7	1.30×10^{-3}	25°C, 95% RH		*J. Am. Chem. Soc.* **2018**,
	2.30×10^{-3}	50°C, 95% RH		140, 13156–13160
KAUST-7'	6.70×10^{-3}	25°C, 95% RH		*J. Am. Chem. Soc.* **2018**,
	1.10×10^{-2}	50°C, 95% RH		140, 13156–13160
DNA@ZIF-8-3/25	3.40×10^{-4}	25°C, 97% RH	0.86	*Adv. Mater.* **2018**, 30,
	1.70×10^{-1}	75°C, 97% RH		1705155–1705162
Co-tri	2.92×10^{-2}	40°C, 98% RH	0.40	*Angew. Chem. Int. Ed.*
	1.49×10^{-1}	80°C, 98% RH		**2018**, 57, 6662–6666
				the highest among CPs/MOFs/COFs
Co-tetra	1.38×10^{-2}	40°C, 98% RH	0.29	*Angew. Chem. Int. Ed.*
	4.15×10^{-2}	80°C, 98% RH		**2018**, 57, 6662–6666
Co-fdc	9.54×10^{-4}	40°C, 98% RH	0.40	*Angew. Chem. Int. Ed.*
	4.85×10^{-3}	80°C, 98% RH		**2018**, 57, 6662–6666
MOP-1	1.41×10^{-3}	30°C, 98% RH	0.225	*J. Mater. Chem. A.* **2018**, 6,
	2.79×10^{-3}	60°C, 98% RH		7724–7730
Na$_2$[Eu(SDB)$_2$(COO)] 0.375DMF·0.4H$_2$O	2.91×10^{-2}	30°C, 90% RH	0.10	*Chem. Commun.* **2018**, 54,
	8.78×10^{-3}	90°C, 90% RH		4429–4432
(DMA)$_3$[Zr(HL)F$_2$]	8×10^{-3}	70°C, 95% RH	0.20	*Chem. Mater.* **2018**, 30,
PCMOF20	1.3×10^{-2}	85°C, 95% RH	0.26	314–318
JLU–Liu44	8.40×10^{-3}	27°C, 98% RH	0.25	*Cryst. Growth Des.* **2017**, 17, 3556–3561
(N$_2$H$_5$)[CeEu(C$_2$O$_4$)$_4$(N$_2$H$_5$)]·4H$_2$O	3.42×10^{-3}	25°C, 100% RH	0.10	*Adv. Mater.* **2017**, 29, 1701804–1701809
3a	1.35×10^{-5}	20°C, 98% RH	1.00	*Chem. Eur. J.* **2017**, 23,
	3.31×10^{-3}	70°C, 98% RH		8980–8986
PCMOF-17	1.17×10^{-3}	25°C, 40% RH	0.31	*J. Am. Chem. Soc.* **2017**, 139, 7176–7179
(Me$_2$NH$_2$)[Eu(L)]	2.17×10^{-5}	30°C, 98% RH	0.72	*J. Am. Chem. Soc.* **2017**,
	3.76×10^{-3}	100°C, 98% RH	0.38	139, 3505–3512
JUC-200	1.62×10^{-3}	80°C, 100% RH		*J. Mater. Chem. A.* **2017**, 5,

				12943–12950
BUT-8(Cr)A	1.27×10^{-1}	80°C, 100% RH	0.25	*Nat. Energy.* **2017**, 2, 877–883
BUT-83	3.90×10^{-2}	80°C, 97% RH	0.34	*J. Mater. Chem. A.* **2017**, 5, 14525–14529
MROF-1	1.72×10^{-2}	70°C, 97% RH		*J. Mater. Chem. A.* **2016**, 4, 18742–18746
VNU-15	2.90×10^{-2}	95°C, 60% RH	0.22	*J. Mater. Chem. A.* **2016**,4, 3638–3641
UiO-66(Zr)-(CO$_2$H)$_2$	2.30×10^{-3}	90°C, 95% RH	0.17	*Angew. Chem. Int. Ed.* **2016**, 128, 3987–3991
NENU-530	1.50×10^{-3}	75°C, 98% RH	0.33	*Chem. Eur. J.* **2016**, 22, 9299–9304
PCMOF-10	3.55×10^{-2}	70°C, 95% RH		*J. Am. Chem. Soc.* **2015**, 137, 7640–7643
Fe-CAT-5	5.0×10^{-2}	25°C, 98% RH		*J. Am. Chem. Soc.* **2015**, 137, 15394–15397
CPM-103a	2.30×10^{-3}	22.5°C, 98% RH		*Angew. Chem. Int. Ed.*
CPM-103a	2.10×10^{-3}			**2015**, 54, 7886–7890
UiO-66(SO$_3$H)$_2$	1.40×10^{-2}	25°C, 90% RH	0.32	*Angew. Chem. Int. Ed.*
	8.40×10^{-2}	80°C, 90% RH		**2015**, 54, 5142–5146
UiO-66-SO$_3$H	3.40×10^{-3}	30°C, 97% RH	0.27	*Cryst. Growth Des.* **2015**,
UiO-66-2COOH	1×10^{-3}	30°C, 97% RH	0.18	15, 5827–5833
PCMOF2$_{1/2}$	2.10×10^{-2}	85°C, 90% RH		*J. Am. Chem. Soc.* **2013**, 135, 1193–1196
PCMOF-5	4×10^{-3}	62°C, 98% RH	0.16	*J. Am. Chem. Soc.* **2013**, 135, 1193–1196

5. References

1. (a) X. Liu, L. Zhai, W. W. Zhang, J. L. Zuo, Z. X. Yang, X. M. Ren, *Dalton Trans.*, **2017**, 46, 7953–7959; (b) L. Zhai, Z. X. Yang, W. W. Zhang, J. L. Zuo, X. M. Ren, *Inorg. Chem.* **2018**, 57, 4171–4180.

2. M. D. Smith, A. Jaffe, E. R. Dohner, A. M. Lindenberg, H. I. Karunadasa, *Chem. Sci.*, **2017**, 8, 4497–4504.